AIAA 80-0768R

F-16 Flutter Suppression System Investigation Feasibility Study and Wind Tunnel Tests

R. P. Peloubet Jr.,* R. L. Haller,† and R. M. Bolding‡
General Dynamics, Fort Worth, Texas

A study was conducted to determine the feasibility of employing active controls on the F-16 to suppress wing-store flutter for several external store configurations. It was determined that the existing flaperons, with modifications to the integrated servoactuators, were effective in suppressing flutter. The F-16 flutter model was tested with active flaperons. Open-loop frequency response functions (FRF's) were successfully measured in the wind tunnel environment both with the feedback loop physically opened and with the loop closed. These measurements provided guidance in the selection of sensor locations and feedback control laws to suppress flutter. Control law variations were made to obtain the desired FRF characteristics. A 100% increase in dynamic pressure above the flutter dynamic pressure was demonstrated.

Introduction

FIGHTER aircraft are required to carry a very large number of external store configurations. The probability is high that at least a small subset of these configurations will flutter within the desired operational envelope of the airplane. This probability is further increased as new stores are added to the operational airplane inventory. When wing-store flutter problems occur, the solution requires a modification of the airplane (usually a change in stiffness and weight) and/or a speed restriction which reduces the operational envelope of the airplane. Flutter suppression with active controls is another solution which has been investigated in recent years. Several approaches have been taken to design these systems.[1-3]

One of the more promising approaches to the design of calibrated active control systems is the frequency response method. This approach is attractive because of the state of development of methods for computing oscillatory aerodynamic pressure distributions, because frequency response functions (FRF's) are experimentally measurable, and because the military specification for the stability of aeroservoelastic systems is based on the Nyquist criteria. This method was applied in a flutter suppression system (FSS) feasibility study[4] for the F-4. The results of this study indicate that the milder flutter modes and the lower flutter frequencies associated with wing-store configurations could be relatively easily suppressed with active controls. The initial design approach for the active control system for the YF-17 semispan flutter model was the root locus method.[5] However, a modified Nyquist approach was subsequently used.[6] The Nyquist stability criteria has been applied extensively by Turner.[7]

The Nyquist criteria was employed as the principal design tool in the F-16 FSS investigations. For the system with negative feedback shown in Fig. 1, the transfer function for the closed loop system is

$$x_0/x_i = G/(1+GH) \tag{1}$$

The Nyquist criteria can be interpreted to state that a clockwise (cw) encirclement of the $(-1,0)$ point by the open-loop FRF at any speed indicates that the closed-loop system is unstable. Furthermore, above the unaugmented flutter speed, V_f, a counterclockwise (ccw) encirclement of the $(-1,0)$ point is necessary to suppress flutter. Hence the objective in applying the Nyquist criteria to the design of a FSS is to prevent cw encirclement of the $(-1,0)$ point at all speeds, while maintaining a ccw enclosure of that point above V_f.

Wind tunnel tests of the F-16 flutter suppression model, conducted between January 22 and February 8, 1979, were marked by some significant accomplishments in FSS technology. The open-loop FRF was successfully measured in the wind tunnel environment. Furthermore, it was measured, on-line, both below and above V_f. Sensor locations were selected and feedback control laws were developed on the basis of the visibility provided by the measured FRF data. The model was tested to a dynamic pressure (q) that was 100% higher than the flutter q. This paper presents an overview of an F-16 FSS feasibility study, and a description of the wind tunnel tests of the F-16 flutter suppression model.

F-16 FSS Feasibility Study

The Air Force Flight Dynamics Laboratory (AFFDL) sponsored a study§ for determining the feasibility of developing an F-16 FSS[8] that would suppress flutter for several specified external store configurations. Candidate control surfaces were 1) the existing flaperons, 2) a combination of the flaperons and the existing leading-edge flaps, and 3) a new control surface dedicated to flutter suppression. Most of the effort was directed toward the use of the flaperon after it was determined that it was adequate for suppressing flutter.

Three takeoff store configurations and associated downloadings, which were considered in the FSS study, are shown in Table 1. Most of the store configurations had previously been tested in the wind tunnel. The configurations that fluttered were designated as design configurations. The others were designated as off-design configurations. A primary objective of the study was to determine if a FSS could be found that would stabilize each of the design configurations without destabilizing the off-design configurations. Although flight flutter tests had cleared each of the design store configurations to the applicable limit speed, these store configurations were selected for the FSS study because each was known to have fluttered in the wind tunnel.

Presented as Paper 80-0768 at the AIAA/ASME/ASCE/AHS 21st Structures, Structural Dynamics and Materials Conference, Seattle, Wash., May 12-14, 1980; submitted June 4, 1980; revision received April 30, 1981.

*Engineering Chief. Associate Fellow AIAA.
†Senior Engineering Specialist.
‡Senior Structures Engineer. Member AIAA.

§Sponsored by the Air Force Flight Dynamics Laboratory under Contract F33615-77-C-3081.

Analytical Methods

The truncated mode method of analysis[9] was employed. A minimum of 15 flexible modes was combined with the rigid body modes for the frequency response calculations. A three-dimensional doublet lattice representation of the airplane was employed to compute subsonic oscillatory pressure distributions.

Frequency response functions relating sensor response to control surface deflection were computed for a large number of candidate sensor locations. The sensors whose FRF's exhibited the best characteristics were selected for control-law development. Desirable characteristics were a large resonance at the flutter frequency relative to the other resonances and a favorable orientation of the associated loop with respect to the other loops.

The form of the control laws employed by Nissim to relate the control surface feedback to the sensor response is shown in Eq. (2):

$$\delta = (C_1 + iG_1)h/b + (C_2 + iG_2)\alpha \tag{2}$$

Nissim formulated the flutter suppression problem such that the control-law constants (C_i, G_i) were selected with the objective of ensuring that the roots of an eigenvalue problem were positive. A corresponding objective when applying the Nyquist criteria is to select the control law constants that ensure that the ccw loop encloses the $(-1,0)$ point without causing a cw enclosure of the point. The application of this control-law form to the FRF relating sensor response to control surface deflection produces a constant gain and phase-angle change across the frequency range of the function. Although control laws of this form are physically realizable, it is simpler to implement an acceleration-plus-velocity control-law form. The same gain change and phase-angle change can be obtained at a selected reference frequency (ω_r) with an amplifier $(-1/\omega_r^2)$ and an integrator $(1/\omega_r s)$ applied to an acceleration $(\ddot{h})$ sensor.

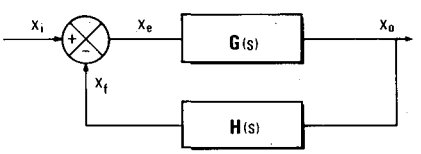

Fig. 1 Block diagram of a closed loop system.

$$\delta = \left(-\frac{C}{\omega_r^2} + \frac{G}{\omega_r s}\right)\frac{\ddot{h}}{b} \tag{3}$$

This control-law form produces a phase-angle change, which is relatively constant in the vicinity of ω_r and spans only 90 deg over the infinite frequency range. The acceleration-plus-velocity control-law form has the desirable characteristic of attenuating the feedback signal at frequencies below ω_r and the undesirable characteristic of amplifying the feedback signal at the higher frequencies.

The integrated servoactuator (ISA) acts as a low-pass filter. Its no-load, no-flow FRF is represented by a fourth-order transfer function.

$$H_A = \left(\frac{2925}{s^2 + 165s + 2925}\right)\left(\frac{5098}{s^2 + 105s + 5098}\right) \tag{4}$$

A high-pass filter, Eq. (5), was used in the FSS feedback loop to prevent adverse coupling between the FSS and the basic flight control system (FCS).

$$H_{hp} = s/(s+20) \tag{5}$$

It might seem that the FRF's relating individual sensor response to control surface deflection could have been enhanced with a low-damped, second-order filter tuned to the flutter frequency. This is indeed true at speeds below V_f. However, above V_f, the rapid increase in phase lag at the tuned frequency has the effect of collapsing the ccw loop and thus reducing the phase margin available in the unfiltered signal.

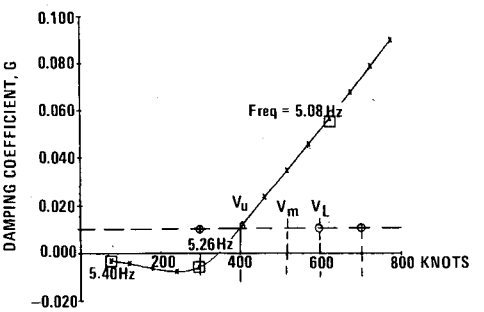

Fig. 2 Structural damping vs velocity for feasibility study wing-store configuration 33.

Table 1 Feasibility study takeoff loading and downloading

	Configuration	Wing station 71	120	157	Tip	Wind tunnel tested	Wind tunnel flutter point[a]	Limit speed
Task I								
Takeoff loading	11	Tank (full)	...	AIM-9	AIM-9	Yes	No S&A	Tank
	12	Full	...	AIM-9	...	Yes	Yes (S, 6.8)	Tank
	13	½(CBE)[b]	...	AIM-9	...	No	No S&A	Tank
	14	½(CBE)	...	...	AIM-9	Yes	No S&A	Tank
	15	...	...	AIM-9	AIM-9	Yes	Yes (S,8.8)	Clean
	16	...	...	AIM-9	...	Yes	No S&A	Clean
	17	...	...	...	AIM-9	Yes	No S&A	Clean
Task II								
Takeoff loading	21	Tank (full)	ECM-12	...	AIM-9	No	No S&A	Tank
	22	...	ECM-12	...	AIM-9	Yes	Yes (S,9.0)	Clean
	23	...	ECM-12	...	...	Yes	Yes (S,9.2) (A,10.5)	Clean
Task III							No S&A	
Takeoff loading	31	Tank (full)	GBU-8B	...	AIM-9	Yes	Yes (A,5.3)	GBU-8B
	32	...	GBU-8B	...	AIM-9	Yes	Yes (A,5.3)	GBU-8B
	33	½(CBE)	GBU-8B	...	AIM-9	Yes	Yes (A,5.4)	GBU-8B

[a] Frequencies are airplane scale. [b] Center bay empty.

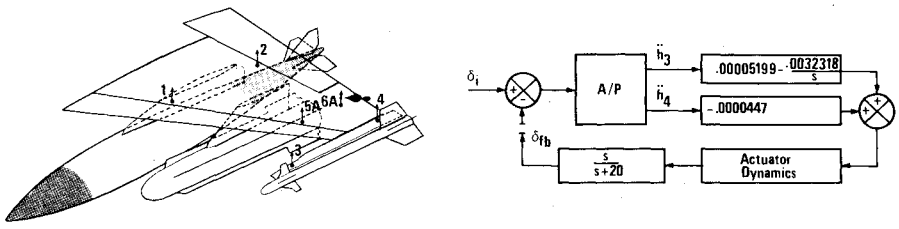

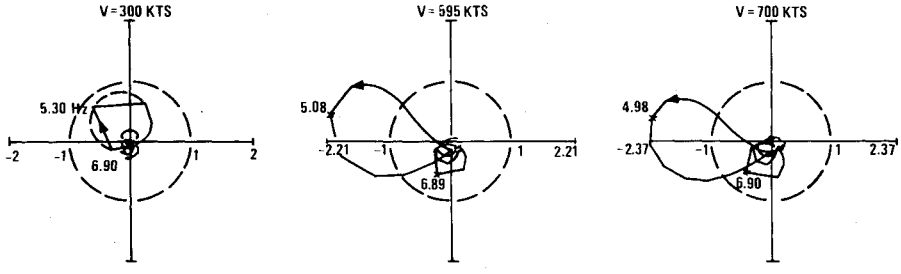

Fig. 3 Feasibility study flutter suppression system 28 and open-loop frequency response functions for wing-store configuration 33.

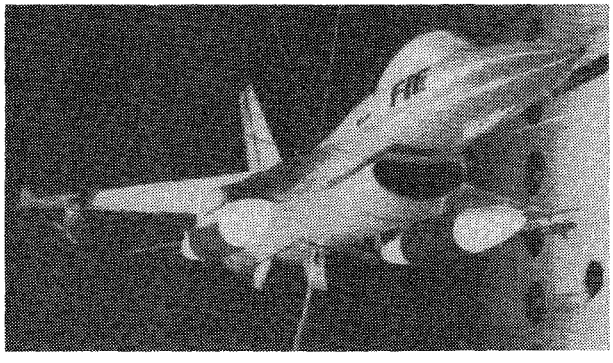

Fig. 4 ¼-scale F-16 FSS model (IRAD wing-store configuration) in NASA LRC 16-ft Transonic Dynamics Tunnel.

Table 2 Model scale ratios

Parameter	Model/airplane
L, length	1/4
q, dynamic pressure	1/8.04
M, Mach number	1
a, speed of sound	1/2.19
V, velocity	1/2.19
k, reduced frequency	1.2
ω, frequency	1.522
ρ, fluid density	1/1.678
m, mass	1/107.41

FSS Development

The manner in which an FSS control law was developed for configuration 33 (Table 1) will illustrate the method used for all of the store configurations. The results of a conventional antisymmetric flutter analysis of this configuration, at Mach 0.9 and sea level altitude, is shown in Fig. 2. The flutter mode can be described as a coupling between the first and second natural modes. The first mode (5.1 Hz) is characterized by wing bending and GBU-8 pitch. The second mode (5.4 Hz) is characterized by AIM-9 pitch. The computed unaugmented flutter speed, V_u, assuming 0.01 structural damping, is approximately 400 knots. The airplane scale flutter velocity obtained in earlier wind tunnel tests is indicated by V_m. The limit speed dictated by GBU-8 carriage is V_L. The objective of the FSS design was to obtain a computed augmented flutter speed, V_A, such that

$$V_A \geq V_u 1.2 V_L / V_m \tag{6}$$

Open-loop FRF's were computed for the three speeds indicated in Fig. 2, assuming 0.01 structural damping in each natural mode. Each FRF relating sensor response to control surface deflection was combined with the ISA and high-pass filter transfer functions. From these FRF's, two sensor locations were selected for FSS development. In this case, sensors located at the forward and aft ends of the tip launcher were selected. The control-law constants for each sensor were selected such that the ccw loop of the FRF at a selected speed above V_u was located with its resonance at the (-1,0) point. The response of the two conditioned FRF's were summed to give a resonance at the $(-2,0)$ point. An iterative process ensued in which each of the control-law constants was perturbed and the phase and gain margins were maximized. An HP9830 minicomputer and a plotter facilitated this process by presenting the results graphically for immediate evaluation by the analyst. FSS 28 was developed for configuration 33 by this process.

The block diagram for FSS 28 is shown in Fig. 3 along with the open-loop feedback FRF for three speeds. Each of the Nyquist plots has a compound, linear magnitude scale. All magnitudes greater than unity are scaled such that the maximum magnitude is twice the unit circle distance from the origin. At 300 knots (i.e., below V_u) the Nyquist plot has only cw loops. The flutter loop near 5.3 Hz has a resonant phase angle slightly greater than 90 deg. However, as the speed approaches V_u, the resonant phase angle rotates in the cw direction and approaches a phase angle near 0 deg. Above V_u the flutter loop becomes a ccw loop. At 595 and 700 knots (both above V_u), the ccw loop encloses the $(-1,0)$ point indicating that the closed-loop FSS suppresses flutter.

An FSS was developed in this manner for each design store configuration and then tested on other design and off-design configurations. It was found that an FSS could be obtained for each design configuration that produced the desired increase in flutter speed. However, a single FSS which would perform satisfactorily for all design configurations could not be found. Furthermore, many of the FSS's would destabilize one or more of the off-design configurations.

Feasibility Study Conclusions

The flaperon can be used as an active control surface to suppress flutter for all of the store configurations studied. For application to an operational F-16, the integrated servoactuator (ISA) would need to be modified to increase its hinge moment capability and to increase the available flaperon deflection in the 5-10 Hz frequency range. The control laws for the FSS and possibly the sensor locations will have to be scheduled as a function of store configuration and

Table 3 Airplane ISA and model servoactuator

Characteristic	Full-scale ISA	Model-scale ISA	Model servoactuator
Break frequency (no load, no flow)	3	4.6	27
Rate limit (deg/s)	52	80	1342
Maximum hinge moment (ft-lb)	1.7×10^4	330	294
Hydraulic stiffness (ft-lb/rad)	7.68×10^5	1035	4930

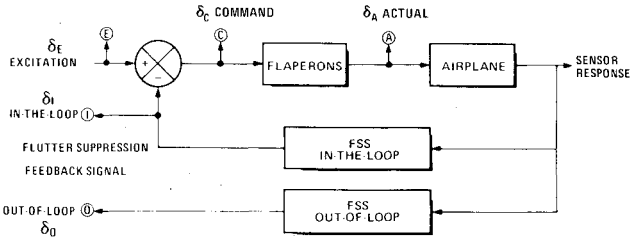

Fig. 5 Block diagram of the wind tunnel test flutter suppression system configuration.

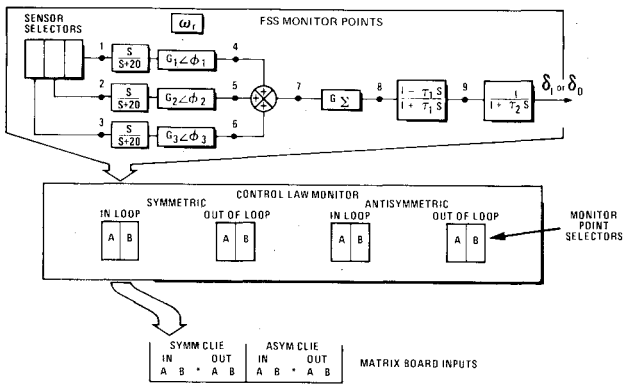

Fig. 6 Flutter suppression system monitor.

flight condition. The FSS control laws and sensor locations could be stored in an FSS computer as a function of flight condition and external store configuration. The flight condition can be identified by the F-16 air data computer, and the store configuration can be identified by the F-16 store management system. In view of the uncertainties associated with computing the FRF relating sensor response to control surface deflection over a range of store configuration and flight conditions, it will be necessary to measure FRF data to determine the most effective sensor locations and control laws before storing this data in the FSS computer.

F-16 FSS Flutter Model Tests

The ¼-scale F-16 flutter model has been used extensively in the F-16 flutter clearance program. Having made five entries in the NASA Langley Transonic Dynamics Tunnel (TDT), the model is a mature test vehicle with demonstrated durability and reliability. In its free-flying test configuration (Fig. 4), the model flies on two cables—a drag cable, which passes horizontally through pulleys in the model and extends forward to the tunnel walls, and a stabilizing cable, which passes vertically through pulleys in the model and extends aft to the tunnel floor and ceiling. A four-cable snubber system provides emergency restraint and is used to hold the model when it is not flying. The model is flown by a pilot in the control room who commands the position of the all-movable horizontal tails.

The ultimate objectives of the FSS tests were to install store configurations that had previously fluttered, reestablish the flutter boundary, develop and activate the FSS, and continue testing within the unaugmented flutter region. However, there were several intermediate objectives which were directed toward answering questions with respect to the testing technique and with respect to performing the tests on a full-span, free-flying model, such as

1) determining if the frequency response characteristics of the left and right actuators were sufficiently matched to ensure that when a symmetric random command signal was applied, the antisymmetric component of the actuator deflections was small compared with the symmetric component, and vice versa;

2) determining if the averaged sum and difference of the signals from accelerometer pairs located symmetrically with respect to the model centerline could be used to separate symmetric and antisymmetric components;

3) determining if the open-loop FRF could be measured with sufficient accuracy to be useable, recognizing that the wind tunnel turbulence level could not be controlled and hence the signal-to-noise ratio would be limited by the control surface excitation level that could be commanded without losing control of the model;

4) determining if the act of switching from one FSS (set of sensors, control laws, and filters) to another could be accomplished without causing dangerous transient model motion or trim alterations; and

5) determining if a symmetric and an antisymmetric FSS could be implemented simultaneously. This capability would be needed if one type of flutter was encountered while the other type was being suppressed.

Flutter Model Modifications

The F-16 flutter model is designed for testing in freon with 20% margin in flutter velocity. Model scale ratios are given in Table 2. The major changes to the model for the FSS tests consisted of the installation of a new set of wings and the installation of a hydraulic system in the fuselage. Each wing was instrumented with six accelerometers. The hydraulic system was used to power the model flaperon servoactuators. The servoactuators were independently controlled and were not designed to be dynamically similar to the full-scale ISA as indicated by the comparison in Table 3.

The variable break frequency (−3-dB point) was set at 27 Hz initially and later reduced to 17 Hz. To ensure linear response for large commanded deflections at higher frequencies, the model servoactuator was designed to have a very high rate limit. The stall hinge moment is very near to the model scale value. The hydraulic stiffness of the servoactuator is considerably higher than the scaled ISA stiffness. However, the stiffness of the flaperon actuator shaft was tuned to produce the correct scaled flaperon rotational frequency. The measured FRF's for the two actuators (ratio of actuator deflection to the commanded deflection) were matched to within 0.5 dB and a 13-deg phase angle from 0 to 25 Hz.

Model Ground Tests

Ground vibration tests were conducted on the modified model without hydraulic power but with the actuators mechanically locked and again with the actuators unlocked and hydraulically energized. The two sets of natural frequencies and mode shapes were virtually identical. Both sets of data compared favorably with ground vibration data

for the unmodified model, which indicated that the modifications had not significantly changed the dynamic characteristics. Additional tests were conducted in which the FRF relating acceleration response to flaperon deflection was measured with the SD-360 real time analyzer in the same manner planned for the wind tunnel test.

FSS Control and Monitoring Systems

A pair of the control systems, shown in Fig. 5, were developed for the model—one for symmetric control and another for antisymmetric control. The symmetric (left + right) and antisymmetric (left − right) response of the six accelerometer pairs were used for FSS purposes, although the individual accelerometer responses could also be monitored. Similarly, control surface signals were processed by the FSS as symmetric and antisymmetric signals and converted to left and right signals for individual servoactuators. The particular control system data available for analysis included the excitation δ_E, command (closed-loop error signal) δ_C, and actual control surface deflection (actuator displacement transducer output) δ_A, signals. Two parallel FSS feedback loops were used. The feedback signal for the in-the-loop FSS, δ_I, and the feedback signal for the out-of-the-loop, δ_O, could also be monitored. After the FRF for the out-of-the-loop FSS was measured and checked for stability, the two FSS's could be interchanged with the push of a button.

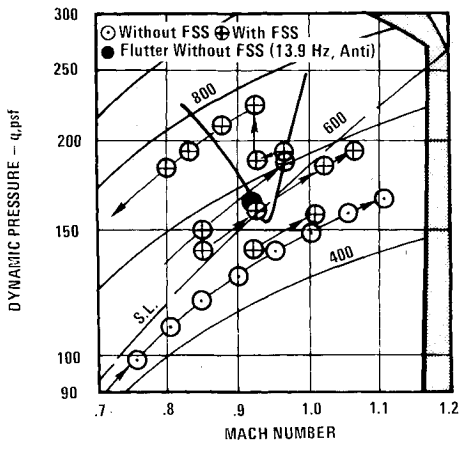

Fig. 7 Wind tunnel test points for the IRAD wing-store configuration.

Each of the four FSS's is described by the block diagram in Fig. 6. Any combination of three signals from the six available sensor pairs could be selected at anytime for use in a particular FSS.

FRF Measurement Procedure

At selected, stabilized, wind tunnel test conditions, the flaperons were excited either symmetrically or antisymmetrically with a band-passed pseudo-random excitation signal. The excitation amplitude was increased slowly until the model response was sufficient to produce an acceptable FRF or until further increase in the model response was judged to be unsafe by the test director or the pilot. The maximum excitation levels that were applied produced random flaperon deflections with maximum peaks of approximately +2 deg. The data acquisition time was a compromise between a desire to average FRF data from a large number of records for accuracy and wind tunnel test time limitations. Typically, the SD-360 was used to average 32 FRF's obtained from 32 records with a 75% overlap (i.e., eight independent records) over an analysis range of 0.1-51.2 Hz in 0.1-Hz increments, which required an acquisition time of 80 s.

By use of this procedure, numerous FRF's were measured during wind tunnel runs. Many additional FRF's were measured between wind tunnel runs by playing back data recorded on magnetic tape, through the control-law system. This process provided a means of selecting alternate sensor and feedback laws to be tried in subsequent wind tunnel runs.

The development and the success of the FSS control laws are illustrated by describing the test data for two of the store configurations that were tested. These are the independent research and development (IRAD) store configuration and configuration 33 (Table 1). The IRAD store configuration has a half-full fuel tank (center bay full) at station 71 and an AIM-9 at 157.

IRAD Store Configuration Tests

Wind tunnel test points for the IRAD configuration are shown in Fig. 7. Flutter tests of the unaugmented model were initially conducted along a nominally constant pressure head of 450 lb/ft^2. Testing was conducted at successively higher pressure heads until flutter was encountered at Mach 0.925 and 158 lb/ft^2 dynamic pressure (q). The flutter boundary was further defined by a point at Mach 0.92 and a q of 166 lb/ft^2. The flutter mode was antisymmetric at 13.9 Hz.

At Mach 0.88 and a q of 156 lb/ft^2, a point below the flutter boundary, open-loop FRF's were measured by use of

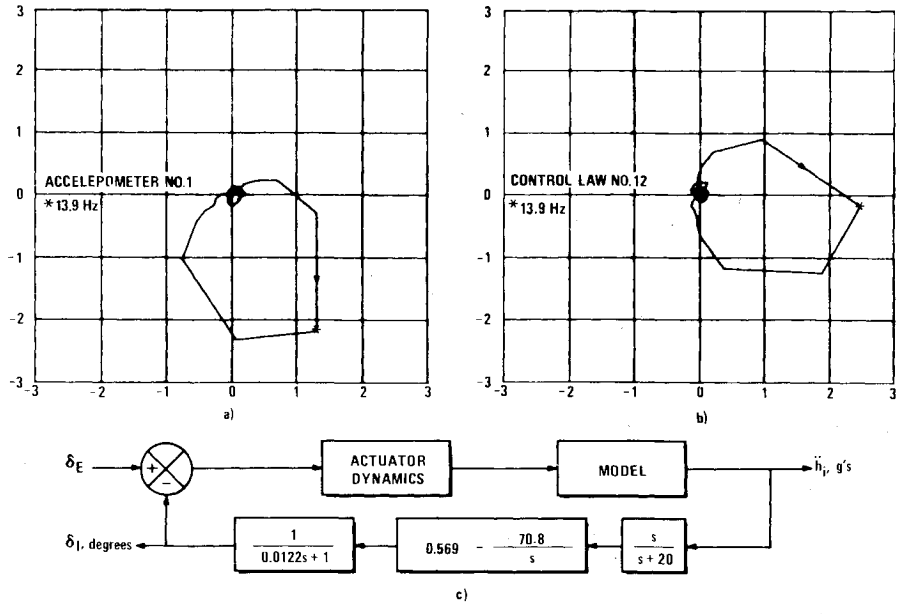

Fig. 8 IRAD wing-store configuration ($M = 0.88$, $q = 157$ lb/ft^2; a) measured open-loop frequency response function for antisymmetric accelerometer No. 1, b) measured open-loop frequency response function for control law 12 FSS feedback, and c) block diagram of control law 12.

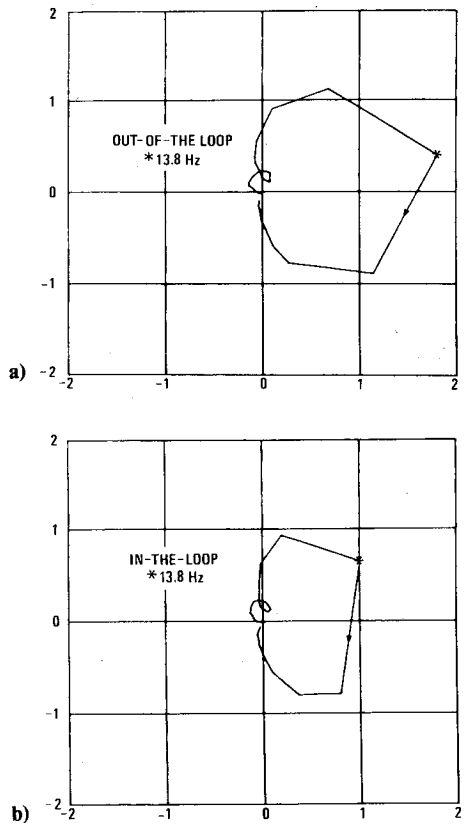

Fig. 9 IRAD wing-store configuration ($M=0.80$, $q=183$ lb/ft^2), control law 11 FSS feedback; measured open-loop frequency response function with a) the feedback loop open and b) the feedback loop closed.

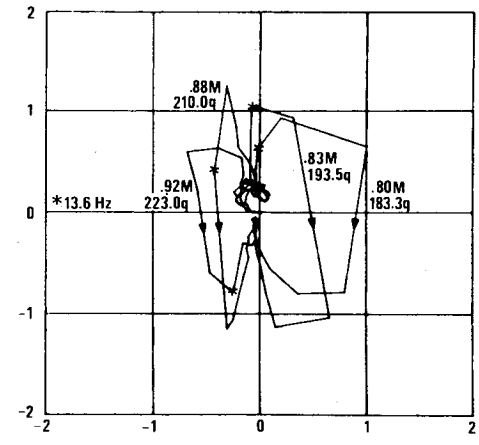

Fig. 10 IRAD wing-store configuration, control law 12 FSS feedback; open-loop frequency response function measured above and below the flutter dynamic pressure.

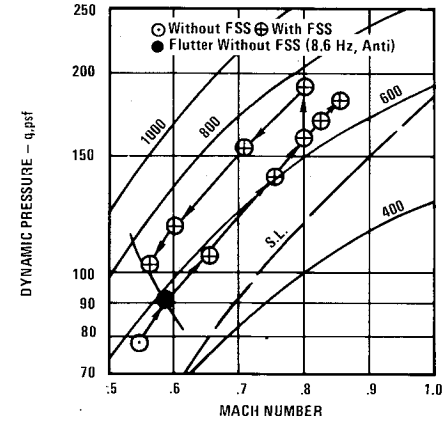

Fig. 11 Wind tunnel test point for wing-store configuration 33.

the out-of-the-loop feedback loop while the gains in the in-the-loop feedback loop were set at zero. The open-loop FRF was measured for each of the six antisymmetric acceleration signals with the high- and low-pass filter in the feedback loop and with the gain set to 1.00 with no phase change at the flutter frequency. As shown in Fig. 8a, the antisymmetric FRF for accelerometer No. 1 exhibited small cw loops relative to the cw loop in the vicinity of the flutter frequency. The control-law gain and phase angles were selected to center the loop on the positive real axis with a resonant magnitude of approximately two. The FRF was remeasured to confirm that the desired effect had been produced, as shown in Fig. 8b. The block diagram for the FSS, labeled as control law 12, is shown in Fig. 8c.

Control law 12 was engaged (by interchanging the two loops), and the open-loop FRF was measured at each of the points indicated in Fig. 7. When the test condition was within the unaugmented flutter region, the ccw loop was always clearly visible on the FRF plot. When the test point was outside the unaugmented flutter region, all loops were clearly cw. Hence, when the model's flight path traversed the flutter region and emerged on the back side of the flutter region, the Nyquist plots provided clear visibility that the model was no longer operating in the unaugmented flutter region. Both sides of the flutter boundary could be clearly identified.

Far from the flutter boundary, the open-loop FRF's measured with the loop physically open and with the loop physically closed are essentially the same across the measured frequency range. Near the flutter boundary, plots of the two FRF's are virtually identical except for the maximum magnitudes in the vicinity of the flutter frequency. A comparison of the open-loop FRF's measured both ways for control law 12 at Mach 0.8 and a q of 183 lb/ft^2 is shown in Fig. 9. Characteristically, the magnitude in the vicinity of the flutter frequency is reduced when the measurement is made with the loop physically closed, near the flutter boundary. The reason for this reduction can be seen by referring to Fig. 1. Near the flutter speed and flutter frequency the open-loop FRF, $G(i\omega)H(i\omega)$, approaches infinity because the $G(i\omega)$ function approaches infinity. When the loop is physically open, the feedback signal, x_f, approaches infinity. Hence the part of x_f that is produced by the input signal is very large compared with the part of x_f that is produced by wind tunnel noise. Therefore the signal-to-noise ratio for x_f is very high. Since the input signal has no error source, the ratio x_f/x_i has a high signal-to-noise ratio and the coherence function is close to unity in the vicinity of the flutter frequency and flutter speed, indicating a high confidence level in the accuracy of the measured FRF. However, when the feedback loop is closed, the feedback signal remains finite near the flutter frequency and flutter speed. Since the open-loop FRF is then measured as the ratio (x_f/x_e), it is clear that the function approaches infinity because the error signal approaches zero, in the absence of noise sources. That is, the feedback signal cancels the input signal to yield a zero error signal. If the feedback signal has a noise component, such as a component due to wind tunnel turbulence, then it does not cancel the input signal, and the error signal has a low signal-to-noise ratio. Hence the maximum distortion always appeared near the flutter frequency and flutter speed and always had the effect of reducing the magnitude of the FRF. The coherence function always had a sharp notch at that point, indicating a low confidence level in the measured FRF at that point. Nevertheless, as shown in Fig. 10, it was always possible to determine whether a resonant loop was cw or ccw. These functions were measured at the four points on Fig. 7 that were measured along a head pressure of approximately 750 lb/ft^2.

Two of the points are below the flutter boundary; two, above the boundary. Although the ccw loops do not enclose the (−1,0) point, because of the distortion at the flutter frequency, the model was clearly stable. At Mach 0.925 the model was tested with control law 12 from a q of 158 lb/ft^2 to 223 lb/ft^2. Even with this 41% increase in q, the model was still stable.

Store Configuration 33 Tests

An unaugmented flutter point for configuration 33 was obtained at Mach 0.59 and a q of 92 lb/ft^2, as shown in Fig. 11. The flutter mode was antisymmetric with a 8.6-Hz frequency. Initially, an analytically developed FSS that utilized sensors 3 and 4 was engaged. This FSS did not produce very large increases in the flutter speed. Large cw loops at other frequencies prevented control-law changes that were needed to improve the performance of the FSS. An examination of the FRF's for the other individual accelerometers revealed that accelerometer 5A had the desired characteristics. Control law 44 was developed with sensor 5A (see Fig. 3).

With control law 44 engaged, the model was tested along a path shown in Fig. 11 to Mach 0.85 and a q of 176 lb/ft^2. There was no indication of impending flutter at that point, but the model was beginning to exhibit a low-frequency dutch-roll type of motion, which prevented further testing along that path. At Mach 0.8, the model was tested along a constant Mach number path to a q of 185 lb/ft^2, where the tests were again terminated because of difficulty in flying the model, although the FSS was still effective in suppressing flutter. The ratio of the 185 lb/ft^2 q at Mach 0.8 to the unaugmented flutter q of 92 lb/ft^2 at Mach 0.59 yields a 100% increase in q because of the FSS. If the unaugmented flutter boundary at Mach 0.8 had been determined, the q increase, based on a constant Mach number comparison, might have been shown to be even higher.

Wind Tunnel Test Conclusions

The open-loop FRF was successfully measured in the wind tunnel environment both with the feedback loop physically open and with it physically closed. In the latter case, wind tunnel turbulence caused a distortion of the FRF in the vicinity of the flutter frequency, which became more pronounced as the unaugmented flutter boundary was approached.

The technique, separating the sensor response into symmetric and antisymmetric components to provide feedback to separate symmetric and antisymmetric FSS's, was very satisfactory. The quality of the measured open-loop FRF data measured in the wind tunnel was better than the zero-airspeed data based on coherence function comparisons and on a comparison of the cross-response to the mutual response. Therefore the response characteristics of the two actuators were adequately matched and the aerodynamic loads produced by the flaperons were more effective in producing a high forcing function than were the zero-airspeed inertia loads. At no time was it necessary to suppress two types of flutter simultaneously. Analytically developed control laws, in general, had to be gain and phase changed on the basis of wind tunnel measured data. In some cases, wind tunnel data were utilized to select different sensor locations. The location of the flutter frequency loop on the Nyquist plots could be seen to rotate with changing wind tunnel conditions. Hence the experimental data confirmed the need for gain and phase scheduling as a function of flight condition to maximize the FSS effectiveness. The control laws were successfully changed in the wind tunnel both below and above the flutter speed without causing objectionable model transient motion.

Flaperon deflection peaks, required to suppress flutter in the wind tunnel environment, never exceeded ±0.6 deg. Random deflections of the flaperon with peak values of approximately ±2 deg were adequate to achieve acceptable FRF measurements.

The model with the IRAD store configuration was tested to a dynamic pressure that was 41% above the flutter dynamic pressure, based on a constant Mach number path. The model with store configuration 33 was tested along a varying Mach number path to a dynamic pressure that exceeded the flutter dynamic pressure by 100%. In both cases, the FSS was still effective at the maximum test conditions.

References

[1] Nissim, E., "Flutter Suppression Using Active Controls Based on the Concept of Aerodynamic Energy," NASA TN D-6199, March 1971.

[2] Sandford, M.C., Abel, I., and Gray, D.L., "Development and Demonstration of a Flutter Suppression System Using Active Controls," NASA TR R-450, Dec. 1975.

[3] Roger, K.L., Hodges, G.E., and Felt, L., "Active Flutter Suppression—A Flight Test Demonstration," *Proceedings of the AIAA/ASME/SAE 15th Structures, Structural Dynamics and Materials Conference*, April 1974.

[4] Triplett, W.E., Landy, R.J., and Irwin, D.W., "Preliminary Design of Active Wing/Store Flutter Prevention Systems for Military Aircraft," AFFDL-TR-74-67, June 1974.

[5] Hwang, C., Winther, B.A., and Mills, G.R., "Demonstration of Active Wing/Store Flutter Suppression Systems," AFFDL-TR-78-65, June 1978.

[6] Noll, T.E. and Huttsell, L.J., "Wing Store Active Flutter Suppression—Correlation of Analyses and Wind Tunnel Test Data," *Journal of Aircraft*, Vol. 16, July 1979, pp. 491-497.

[7] Turner, M.R., "Active Flutter Suppression," Flutter Suppression and Structural Load Alleviation Meeting, AGARD-CP-175, April 1975.

[8] Peloubet, R.P. Jr. and Haller, R.L., "Feasibility Study for F-16 Flutter Suppression System," AFFDL-TR-78-113, Sept. 1978.

[9] Peloubet, R.P. Jr., Haller, R.L., Cunningham, A.M., Cwach, E.E., and Watts, D., "Application of Three Aeroservoelastic Stability Analysis Techniques," AFFDL-TR-76-89, Sept. 1976.